Int J Adv Manuf Technol (2016) 87:3051–3058
DOI 10.1007/s00170-016-8734-x

ORIGINAL ARTICLE

Effect of groove distribution in shoulder on formation, macrostructures, and mechanical properties of pinless friction stir welding of 6061-O aluminum alloy

S. D. Ji[1] · X. C. Meng[1] · L. Ma[1] · S. S. Gao[1]

Received: 9 January 2016 / Accepted: 4 April 2016 / Published online: 12 April 2016

Abstract In order to enrich technological storage of pinless friction stir welding (PFSW), four kinds of shoulders with six grooves owning different shapes were designed and manufactured. PFSW experiments of 6061-O aluminum alloy with the thickness of 1.2 mm were performed. The tool with smaller obliquity grooves easily results in the appearance of a kissing bond defect near the bottom of the nugget zone (NZ) owing to longer distance between the end of the groove and the center of the shoulder. Compared with the larger curvature grooves, the rational curvature and obliquity grooves are beneficial to attain a welding joint with small flashes. For the tool with through grooves, flashes also appear on the surface of the middle zone, besides advancing and retreating sides of the joint. Hardness values of NZ using four kinds of pinless tools are higher than base metal (BM) and the lowest value occurs in the heat-affected zone (HAZ). For the defect-free joints, the tensile specimens all fracture at the HAZ.

Keywords Pinless friction stir welding · 6061-O aluminum alloy · Groove distribution · Macrostructure · Mechanical properties

✉ S. D. Ji
superjsd@163.com

[1] Faculty of Aerospace Engineering, Shenyang Aerospace University, No.37 Daoyi South Avenue, Daoyi Development District Shenyang 110136, China

1 Introduction

As a solid state welding technique, friction stir welding (FSW) has been widely used to weld all series of aluminum alloys because of advantages of high joint quality, non-pollution, low residual stress, and small distortion [1–3]. During the FSW process, a rotational tool composed of a shoulder and pin is plunged into workpieces and frictions with materials, which generates frictional heat and then softens materials to be welded [4]. However, owing to the pin, FSW defects such as cavity and tunnel often appear because of insufficient material flow behavior, deteriorating to mechanical properties of the joint. In addition, after welding, a keyhole forms at the end of joint with the retraction of the rotational pin, which is also detrimental to the bearing capability and corrosion performance in service. Therefore, pinless friction stir welding (PFSW) was developed by researchers at home and abroad in order to eliminate the adverse effects induced by the pin [5–13]. During traditional FSW process, frictional heat is generated by friction between the rotational tool and workpieces to be welded. Frictional heat is mainly provided by shoulder, while frictional heat of the pin is considered to be less than 20 % of total heat input [5–7]. Meanwhile, Tang et al. stated that the peak temperature obtained by using a “Pinless” tool experienced a reduction of about 4 % compared with that using a “Pin” tool [8]. These results are better proof that the pin plays a less influence on heat input. Tozaki et al. developed a “Pinless” tool with scroll groove on the shoulder surface and successfully performed friction stir spot welding of 6061-T4 aluminum alloy [9]. Li et al. employed a tool with involute grooves on the shoulder to weld 1.5-mm-thick 2024-T3 aluminum alloy plates and found that lazy S was eliminated under rational welding parameters [10]. According to the reported papers, how to optimize the geometry of a pinless tool attracts the attention of researchers. Forcellese et al. used

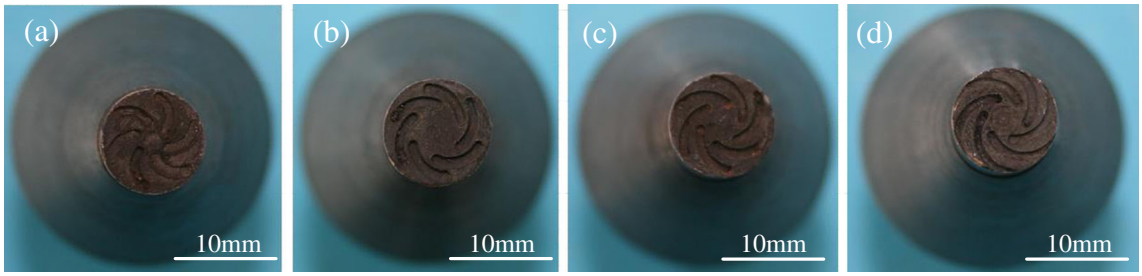

Fig. 1 Four kinds of rotational tools used in the experiment. **a** The large-curvature tool. **b** The small-obliquity tool. **c** The six-groove tool. **d** The through-groove tool

two plane shoulders with different diameters to perform PFSW of AZ31 magnesium alloy and found that increasing shoulder diameter was beneficial to increase the mechanical property of the joint [11]. Bakavos et al. designed a series of "Pinless" tools with different shoulder shape and expounded that material flow was influenced by shoulder shape and then controlled the penetration of the plastic zone into the bottom sheet [12]. Ji et al. also discussed the effect of inner-concave-flute shoulder, concentric-circles-flute shoulder and three-spiral-flute shoulder on joint quality and found that the three-spiral-flute shoulder was the better choice [13].

Generally speaking, it is very important for PFSW to design rational groove on shoulder, but how the groove distribution on the shoulder influences quality of the welding joint is seldom reported. In this paper, in order to enrich technological storage of PFSW, four kinds of pinless tools with different shoulder shapes were designed and manufactured. A 1.2-mm-thick 6061-O aluminum alloy plate was chosen as the research object, which owns excellent extrusion formability, good corrosion resistance, and weldability. Furthermore, effects of groove distribution on formation, macrostructures, and mechanical properties of the joint were investigated in details.

2 Experimental procedure

The base material (BM) employed in this experiment was 6061-O aluminum alloy plate with the thickness of 1.2 mm. The tensile strength and elongation of BM are 129 MPa and 25.7 %, respectively. Four kinds of rotational tools with different shoulder shapes used in this study are shown in Fig. 1. These rotational tools are all made of H13 tool steel and have six curving grooves, whose shoulder diameter, groove width, and groove depth are 10, 1, and 0.5 mm, respectively. Importantly, the length and curvature of the groove of these tools are different, as indicated in Fig. 1. In order to ease the analysis, these four tools are, respectively, named according to the features of groove geometry and distribution. The pinless tool in Fig. 1c is named the six-groove tool. The other three tools are, respectively, named the large-curvature tool (Fig. 1a), the small-obliquity tool (Fig. 1b), and the through-groove tool (Fig. 1d) according to the difference from the six-groove tool in Fig. 1c. The lengths of the groove of the large-curvature tool, the small-obliquity tool, the six-groove tool, and the through-groove tool are approximately 4, 5, 5, and 6 mm. And the radius of the curvature of the groove of the large-curvature tool, the small-obliquity tool, the six-groove

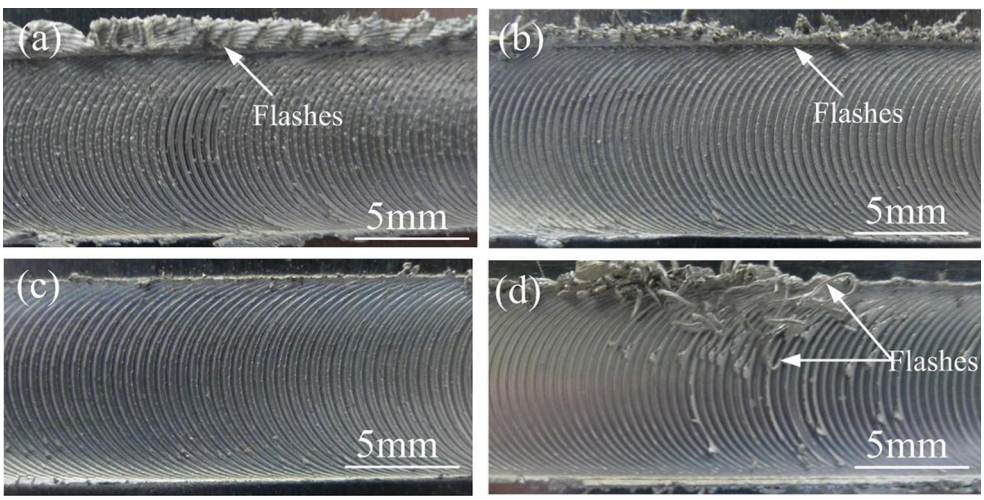

Fig. 2 Surface formation of joints using different rotational tools. **a** The large-curvature tool. **b** The small-obliquity tool. **c** The six-groove tool. **d** The through-groove tool

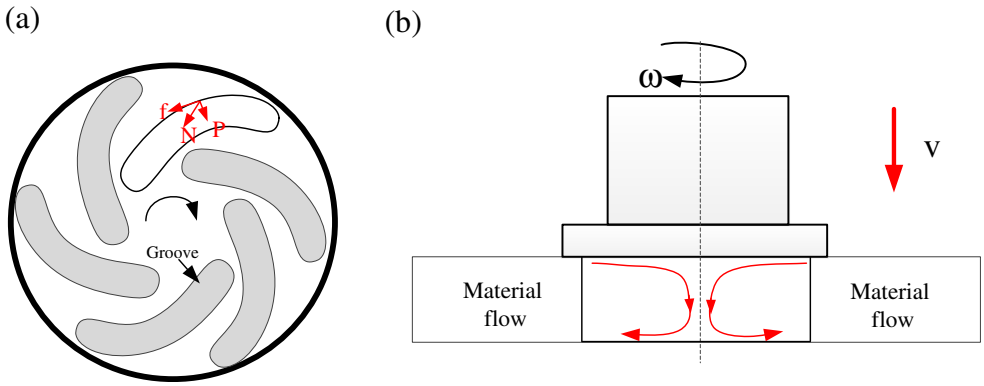

Fig. 3 Schematic illustration of material flow during PFSW process. **a** Interaction forces of plasticized material. **b** Material flow model

tool, and the through-groove tool are about 7, 8.4, 8, and 8 mm. In the experiment, these rotational tools rotated clockwise. In order to decrease the thickness reduction of the joint, the tilt angle with respect to *Z*-axis was chosen as 1.0°. In this study, to investigate the effects of groove distribution on formation and mechanical property of the joint, the optimized welding parameters were used, which were the rotational velocity of 1000 rpm and welding speed of 500 mm/min, respectively. All the experiments were performed using the FSW-3LM-4012 machine. Before welding, surfaces of plates were polished using emery paper and cleaned with acetone in order to wipe off the oxide layer.

After welding, the specimens were cut perpendicular to the welding direction by an electrical discharge cutting machine to perform the mechanical test and macrostructural characterization. The macrostructural features were etched with Keller's reagent (1 ml HF, 1.5 ml HCl, 2.5 ml HNO_3, and 95 ml H_2O) and then observed using an optical microscopy (OLYMPUS, GX71). In order to evaluate the mechanical property of the PFSW joint, three tensile specimens and four bending specimens for each joint were, respectively, prepared according to ISO 4136 and ISO 5173 [14, 15], while the average values were presented for analysis. Meanwhile, tensile test and bending test at room temperature were performed at the crosshead speed of 5 mm/min using a universal tensile machine (Landmark MTS). Micro-hardness of the joint was measured by a micro-hardness tester at a load of 200 g for 10 s under a constant interval of 1 mm.

3 Results and discussion

3.1 Surface formation

Figure 2 shows surface formation of joints using different rotational tools. It can be seen that flashes and arc corrugation

Fig. 4 Macrostructures of joints using different shoulder shapes in cross section. **a** The large-curvature tool. **b** The small-obliquity tool. **c** The six-groove tool. **d** The through-groove tool

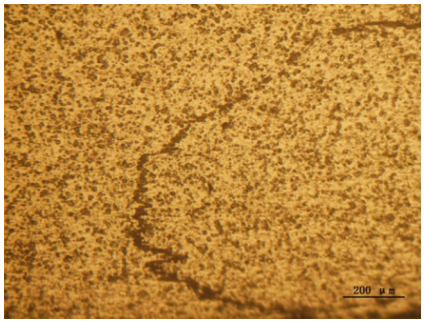

Fig. 5 Partial enlarged picture of kissing bond defect marked by *square* in Fig. 4b

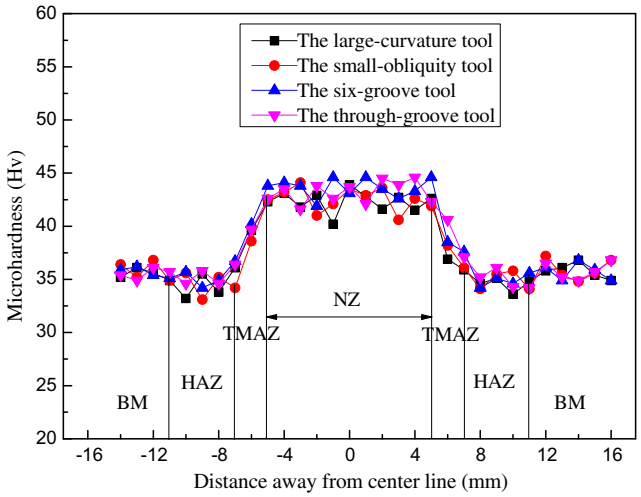

Fig. 7 Hardness distribution of PFSW joint by different pinless tools

form in the surface of PFSW joints, which are also the typical features of the macroscopic morphology of the traditional FSW joint by the rotational tool with pin. During the FSW process, the surface formation of the joint is closely related to heat input and material flow behavior [16]. During the welding process, with the rotation and advancement of the pinless tool, plasticized material flows into the groove of the shoulder continuously. The materials in the groove undergo two forces, which are the positive pressure (p) provided by side wall of groove and the friction force (f) between the plasticized material and side wall of the groove, as shown in Fig. 3a. Therefore, for the pinless tool used in this study, when the tool rotates clockwise, the schematic diagram of material flow behavior is shown in Fig. 3b. In fact, the similar flow model has been talked in the previous papers [9, 17]. It is seen that the plasticized material flows towards the center of the shoulder under the resultant between the positive pressure and friction force and then accumulates at the center of the shoulder. The accumulation materials are more and more during the welding process, and then partly flow downwards according to the law of minimum resistance. Similarly, material near the bottom of the nugget zone (NZ) flows upwards due to the supporting effect of backing plate and the material accumulates near NZ bottom.

Compared with the six-groove tool, the tool in Fig. 1a owns a bigger curvature. Additionally, according to material flow model, the large-curvature groove is thoroughly difficult to transfer plasticized materials from the shoulder edge to shoulder center. More materials easily flow out of the welding joint, consequently causing the bigger flashes, as exhibited in Fig. 2a. Because the end of the groove on the small-obliquity tool (Fig. 1b) is farther away from the center of the shoulder compared with the six-groove tool in Fig. 1c, the similar phenomenon as same as that of the large-curvature tool may appear, which also results in bigger flashes, as indicated in Fig. 2b. With the use of the six-groove tool, the sound surface formation with small flashes was attained (Fig. 2c). This is because the tool in Fig. 1c owns the rational curvature and obliquity, which makes the material in the groove easily flows towards the center of the shoulder. It is interesting that flashes in Fig. 2d form on the middle zone, advancing side (AS), and retreating side (RS) of weld surface, which is different from those in Fig. 2a~c. The materials at the edge of the shoulder easily own higher frictional heat and better material flow. Moreover, according to the continuity law of fluid, the material flowing into the groove owns higher flow velocity. Therefore, plasticized material in the groove near the edge of

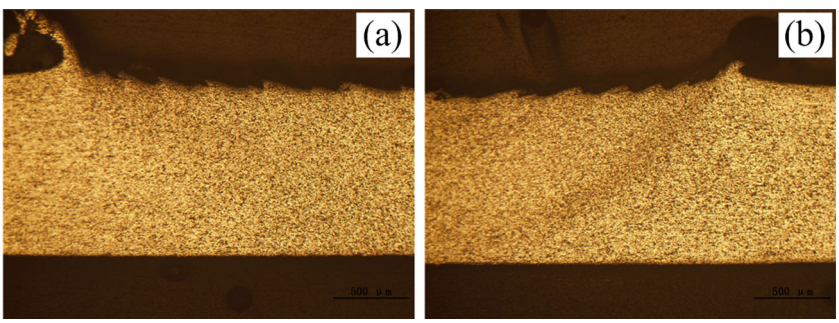

Fig. 6 TMAZ of joint using the small-obliquity tool. **a** RS. **b** AS

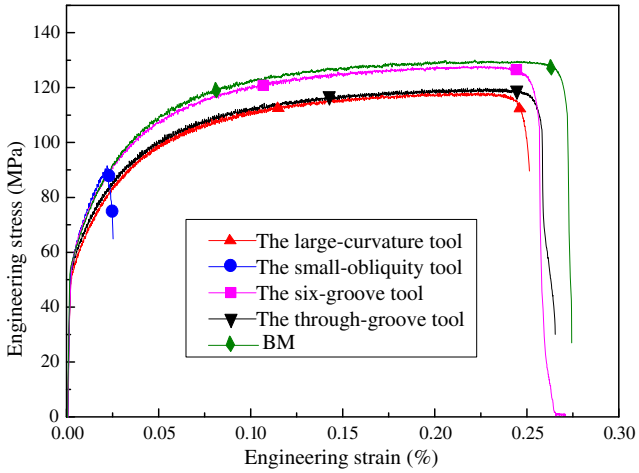

Fig. 8 Engineering stress and strain of joints under different pinless tools

the shoulder easily flows out of the joint along the through groove, which is similar to centrifugal movement and then results in the appearance of flashes in the middle of the weld surface (Fig. 2d).

3.2 Microstructures

Macrostructures of joints under different shoulder shapes are indicated in Fig. 4. Using the large-curvature tool, the six-groove tool and the through-groove tool, sound joints can be obtained and no cavity or tunnel defect appears in these joints (Fig. 4a, c, d). Under the action of three pinless tools, the original interface of two workpieces disappears and then the workpieces are joined together. However, when the small-obliquity tool is used, kissing bond occurs near the bottom of welding joint, as shown in Fig. 4b. The partial enlarged picture of a kissing bond defect is indicated in Fig. 5. For the tools used in this experiment, owing to the existence of the groove, with the rotation and advancement of the pinless

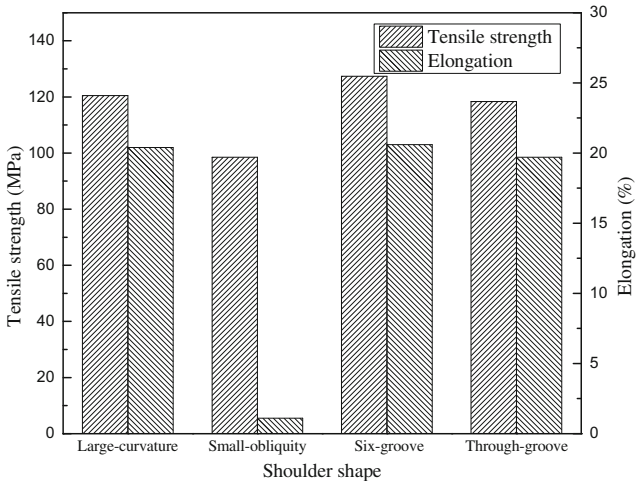

Fig. 9 Tensile strength and elongation of joints under different pinless tools

tool, the plasticized material flows into the inlet and then flows out of the outlet. For PFSW, the material near the shoulder owns higher temperature and the material under the shoulder is heated only by thermal conduction. The temperature of the material decreases with the increase of distance away from the shoulder, leading to higher flow stress. For the material contacting the shoulder, frictional heat input increases with increasing the distance away from the shoulder center, resulting in the lowest flow stress of material under the shoulder edge [13]. Moreover, the end of the groove in the small-obliquity tool is far away from the center of the shoulder. According to the law of minimum resistance, the material accumulated in the outlet easily flows towards the shoulder edge, but not the shoulder center, which easily makes the material near the interface of two workpieces own lower flow velocity, leading to the formation of kissing bond, as indicated in Figs. 4b and 5. Similar to traditional FSW, as shown in Fig. 4a, the PFSW joint is also divided into three zones: NZ, thermo-mechanically affected zone (TMAZ), and heat-affected zone (HAZ) [4]. It is worth mentioning that TMAZ on the AS is clearer than that on the RS, as shown in Fig. 6. This is because the materials in AS undergo bigger shear stress and higher peak temperature compared with that in RS, which are beneficial to plastic deformation of material in AS and then obtain a clear boundary [18]. As indicated in Fig. 4c, the thickness reduction of joint is far less than those in Fig. 4a, b and d, which is attributed to smaller flashes.

3.3 Mechanical properties of joint

As a matter of fact, hardness distribution plays a significant influence on mechanical properties of joint. In this study, hardness distributions of joints under different pinless tools are indicated in Fig. 7. It is observed that the hardness value in the NZ is higher than BM, while the lowest value locates in HAZ. This is attributed to fine and equiaxed grains formed in theNZ because of dynamic recrystallization resulting from higher peak temperature and sufficient material flow [4, 19]. Meanwhile, the material of HAZ only undergoes thermal cycle and does not experience plastic deformation, resulting in coarse grains. According to the formula of Hall-Petch, the finer the grain size, the higher the hardness [20]. Therefore, compared with BM, the hardness values of the NZ and HAZ are higher and lower, respectively.

In this study, tensile tests were performed and engineering stress and strain diagrams of the joint under different pinless tools are shown in Fig. 8. Figure 9 exhibits experimental results of tensile specimens. Obviously, the shape of the pinless tool plays a significant influence on joint quality during PFSW process. It is seen that the tensile strength and elongation of joint using the six-groove tool reach the maximum values of 127.4 MPa and 20.6 %, up to 99 and 80.7 % of BM, respectively. Meanwhile, the mechanical properties of the joint

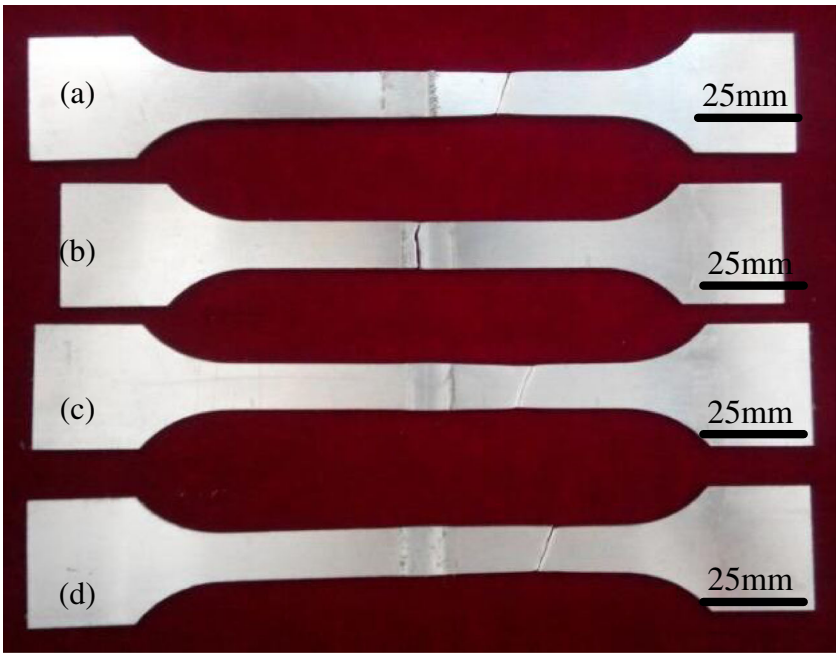

Fig. 10 Fracture locations of tensile specimens obtained using different pinless tools

under the small-obliquity tool are minimum, whose tensile strength and elongation are, respectively, 98.5 MPa and 1.1 %. In fact, joint quality is closely related to the location with minimum hardness and defect location [17]. For the small-obliquity tool used in this experiment, the kissing bond easily becomes crack initiation, which degrades mechanical properties and then results in small plastic deformation of the joint. Because there is no defect appearing in the other three joints, the mechanical properties are decided by the softening zone of the joint [18–21]. Figure 10 exhibits fracture location of joints using different pinless tools. It is seen that the joint of small-obliquity tool fractures at the NZ owing to the kissing defect. For the other three tools, the fracture locations of joints all lie in the region far away from NZ, which may locate near the transition region between HAZ and BM, but not BM. This is because HAZ suffers from higher heat input, which results in the growth of grain, decreasing hardness values [4, 18–23] (Fig. 7).

Surface and root bending specimens of joints under different pinless tools are exhibited in Fig. 11. It is well accepted that if there are defects such as holes or lack of root penetration, the specimen easily fractures at the

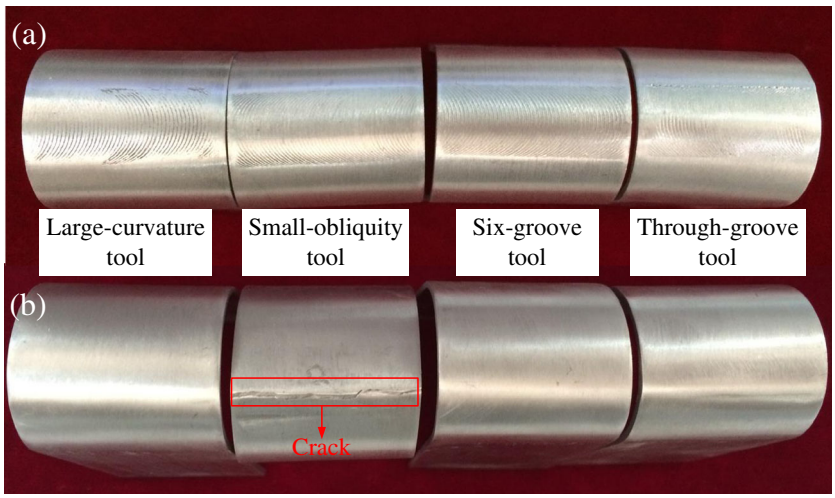

Fig. 11 Surface and root bending specimens of joints under different pinless tools. **a** Surface bending. **b** Root bending

NZ during the bending process [20]. From Fig. 11, it is seen that all the surface bending specimens using different pinless tools reach 180° and crack defect does not occur. However, the crack defect appears in the root bending specimens by the small-obliquity tool, which results from the occurrence of the kissing bond defect, as shown in Fig. 11b. During PFSW process, the frictional heat at the surface of the joint is mainly generated by the shoulder. Therefore, the materials in the surface easily suffer from sufficient heat input and material flow, which is beneficial to diffusion bond of materials and then obtain better joining. However, different from the rotational tool with pin, the material near the bottom of the joint is not stirred by pin for the PFSW process and undergoes heat input by the heat conduction from the top surface. For the small-obliquity tool, the material in the bottom experiences the worse material flow behavior, which is detrimental to the diffusion bond of the materials near the bottom and leads to the formation of the kissing bond defect. Therefore, during a three-point root bending test, the materials in the bottom suffer from tensile stress and stress concentration easily appears owing to the kissing bond, causing the occurrence of a crack (Fig. 11b).

Figure 12 exhibits fracture surface morphologies of typical welding joints. It is seen that there are bigger and deeper dimples on the top and bottom of the joint using the six-groove tool, indicating a typical ductile fracture, as shown in Fig. 12a, b. For the joint using the small-obliquity tool, the dimples with smaller size occurs on the top of the joint (Fig. 12c), while the dimples at the bottom are tiny (Fig. 12d), which means the ineffectiveness of joining. This may be attributed to the occurrence of kissing bond defect.

4 Conclusion

From the viewpoint of enriching technological storage of PFSW, the large-curvature, small-obliquity, six-groove and through-groove tools were designed. Effects of groove distribution on formation, macrostructures, and mechanical properties of 6061-O aluminum alloy welding joint were investigated. Based on the experimental results, the following conclusions can be drawn.

(1) Rational groove curvature and obliquity are beneficial to material flow behavior. The PFSW joint with small flashes can be obtained by the six-groove tool compared with the other three tools. Under the small-obliquity tool, a kissing bond defect easily appears near the bottom of the NZ.

(2) All the surface bending specimens using different pinless tools reach the angle of 180°. The tensile strength and elongation of the welding joint by the six-groove tool reach the maximum values of 127.4 MPa and 20.6 %, equivalent to 99 and 80.7 % of BM, respectively. For the defect-free joints, tensile specimens fracture at the HAZ where the hardness value is lowest.

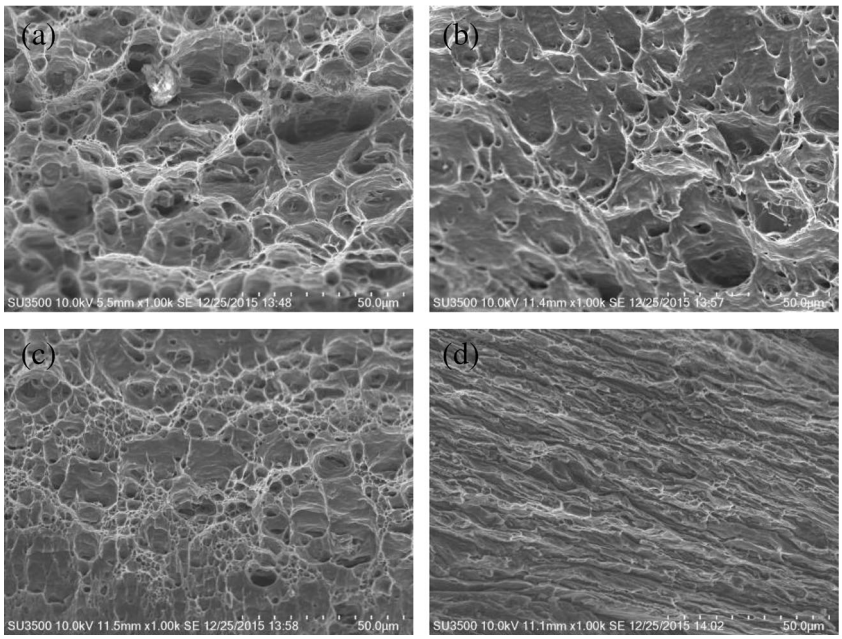

Fig. 12 Fracture surface morphologies of a typical joint. The six-groove tool: (**a**) top of joint and (**b**) bottom of joint; the small-obliquity tool: (**c**) top of joint and (**d**) bottom of joint

Acknowledgment This work is supported by the National Natural Science Foundation of China (No.51204111), the Natural Science Foundation of Liaoning Province (No. 2014024008), the Program for Liaoning Excellent Talents in University (LJQ2015084) and the Aeronautical Science Foundation of China (2014ZE54021).

References

1. Wan L, Huang YX, Lv ZL, Lv SX, Feng JC (2014) Effect of self support friction stir welding on microstructure and microhardness of 6082-T6 aluminum. Mater Des 55:197–203
2. Li JQ, Liu HJ (2013) Design of tool system for the external nonrotational shoulder assisted friction stir welding and its experimental validations on 2219-T6 aluminum alloy. Int J Adv Manuf Technol 66(5-8):623–634
3. Liu HJ, Zhao YQ, Hu YY, Chen SC, Lin Z (2015) Microstructural characteristics and mechanical properties of friction stir lap welding joint of alclad 7B04-T74 aluminum alloy. Int J Adv Manuf Technol 78:1415–1425
4. Mishra RS, Ma ZY (2005) Friction stir welding and processing. Mater Sci Eng R 50:1–78
5. Elangovan K, Balasubramanian V (2007) Influences of pin profile and rotational speed of the tool on the formation of friction stir processing zone in aluminium alloy. Mater Sci Eng A 459:7–18
6. Abbasi Gharacheh M, Kokabi AH, Daneshi GH, Shalchi B, Sarrafi R (2006) The influence of the ratio of "rotational speed/traverse speed" (w/v) on mechanical properties of AZ31 friction stir welds. Int J Machine Tools Manuf 46:1983–1987
7. Forcellese A, Gabrielli F, Simoncini M (2012) Mechanical properties and microstructure of joints in AZ31 thin sheets obtained by friction stir welding using "pin" and "pinless" tool configurations. Mater Des 34:219–229
8. Tang W, Guo X, McClure JC, Murr LE (1998) Heat input and temperature distribution in friction stir welding. J Mater Process Manuf Sci 7:163–172
9. Tozaki Y, Uematsu Y, Tokaji K (2010) A newly developed tool without probe for friction stir spot welding and its performance. J Mater Process Technol 210(6-7):844–851
10. Li WY, Li JF, Zhang ZH, Gao DL, Wang WB, Luan GH (2014) Pinless friction stir welding of AA2024-T3 joint and its failure modes. Trans Tianjin Univ 20(6):439–443
11. Forcellese A, Simoncini M (2012) Plastic flow behaviour and formability of friction stir welded joints in AZ31 thin sheets obtained using the 'pinless' tool configuration. Mater Des 36:123–129
12. Bakavos D, Chen YC, Babout L, Prangnell P (2011) Material interactions in a novel pinless tool approach to friction stir spot welding thin aluminum sheet. Metall Mater Trans A 42A:1266–1282
13. Zhang LG, Ji SD, Luan GH, Dong CL, Fu L (2011) Friction stir welding of Al alloy thin plate by rotational tool without pin. J Mater Sci Technol 27(7):647–652
14. ISO 4136. Destructive tests on welds in metallic materials—transverse tensile test. Geneva: International Organization for Standardization; 2001
15. ISO 5173. Destructive tests on welds in metallic materials—bend tests. Geneva: International Organization for Standardization; 2000
16. Fu RD, Sun RC, Zhang FC, Liu HJ (2012) Improvement of formation quality for friction stir welded joints. Weld Join 91:169–173
17. Ji SD, Meng XC, Zeng YM, Ma L, Gao SS (2016) New technique for eliminating keyhole by active-passive filling friction stir repairing. Mater Des 97:175–182
18. Li DX, Yang XQ, Cui L, He FZ, Shen H (2014) Effect of welding parameters on microstructure and mechanical properties of AA6061-T6 butt welded joints by stationary shoulder friction stir welding. Mater Des 64:251–260
19. Varun Kumar A, Balasrinivasan M (2015) Influence of process parameters on aluminium alloy 6061-o joints by friction stir welding process. Bonfring Int J Indust Eng Manag Sci 5:111–114
20. Ji SD, Meng XC, Li ZW, Ma L, Lu H, Gao SS (2015) Vertical compensation friction stir welding assisted by external stationary shoulder. Mater Des 68:72–79
21. Han B, Huang YX, Lv SX, Wan L, Feng JC, Fu GS (2013) AA7075 bit for repairing AA2219 keyhole by filling friction stir welding. Mater Des 51:25–33
22. Liu HJ, Li JQ, Duan WJ (2013) Friction stir welding characteristics of 2219-T6 aluminum alloy assisted by external non-rotational shoulder. Int J Adv Manuf Technol 64(9):1685–1694
23. Wang FF, Li WY, Shen J, Hu SY, dos Santos JF (2015) Effect of tool rotational speed on the microstructure and mechanical properties of bobbin tool friction stir welding of Al–Li alloy. Mater Des 86:993–940